Robustness Evaluation of Fast Breaker Failure Backup Protection in Bipolar HVDC Grids

M. Wang, W. Leterme*, J. Beerten*, D. Van Hertem**

*Department of Electrical Engineering (ESAT), Division ELECTA & Energyville, University of Leuven (KU Leuven)
Thor Park 8310, 3600 Genk, Belgium Email: mian.wang@kuleuven.be*

Keywords: Breaker failure backup protection, Bipolar HVDC grids, Robustness, Operating conditions, Breaker opening delay.

Abstract

To ensure a reliable fault clearing, a backup protection scheme is required for selective HVDC grid protection. One way to achieve this is to use both voltage and current measurements to distinguish uncleared faults from cleared ones during the fault clearing process of the primary protection. This paper studies the applicability of such a backup protection algorithm in meshed bipolar HVDC grids and evaluates the robustness of the algorithm against system operating conditions and breaker opening delays. The influence of different operating conditions on the fault waveforms is analysed using a three-terminal bipolar test system. The robustness of the fast breaker failure backup protection algorithm is evaluated via simulation studies on the bipolar test system in PSCAD. The simulation results show that the fast breaker failure backup protection algorithm can distinguish between uncleared and cleared faults with sufficient margin for all considered operating conditions.

1 Introduction

For future HVDC grids, the dc protection system is often considered as one of the main challenges due to the difficulty in interrupting a dc current and the stringent time constraint imposed by the fast rising fault current. Although utilizing ac circuit breakers or fault blocking converters to interrupt dc faults might be applicable for small-scale HVDC grids, selective fault detection and fast dc circuit breakers are considered necessary for large-scale meshed HVDC grids [1]. Similar to transmission line protection in ac systems, dc line protections also need primary and backup protection to ensure a reliable fault clearing. Primary protection has to act as soon as the fault is identified within its protection zone, while backup protection should be coordinated properly in case of primary protection failure [2].

In the literature, various protection algorithms have been proposed for both primary protection [3–8] and backup protection [7, 9–11]. Due to the requirement on the operation speed, primary protection algorithms have to operate during the transient stage of the fault, where the fault behaviour can be mainly described by travelling wave phenomenon. The operating time of backup protection on the contrary varies largely, depending on the proposed algorithms. For instance, [7] and [9] propose to compare the current through the primary breaker to a small threshold value after a specific time (20 ms in [9]). This time interval is designed to have sufficient margin to allow the primary protection to clear the fault first. The main disadvantage of these algorithms is the long operation time which results in higher required ratings of dc circuit breakers and larger impact on the dc grid. In [10], a fast breaker failure backup protection algorithm using voltage-current (UI) loci is proposed to quickly detect primary breaker failure, which allow the backup protection to clear the fault within a few milliseconds.

Although the speed of the fast circuit breaker backup protection is superior compared to the simple current criterion based methodologies, the sensitivity of this algorithm to operating conditions and system parameters has not been fully addressed yet. In [10], the analysis was performed taking into account a symmetrical monopolar configuration, further research is needed concerning the applicability of these algorithms in HVDC grids with alternative topologies and parameters. A relay and breaker failure backup protection algorithm using UI loci is investigated including operations during converter or line outages on the same test system in [11]. However, the future HVDC grids can have more complex configurations, such as a bipolar backbone with monopolar tappings [12–14]. First, future bipolar HVDC grids are expected to have intrinsic unbalances, which could be unbalanced power flow or unbalanced configuration due to an outage of a converter, a line or through monopolar tappings. Second, the grounding points and the number of parallel branches connecting to a busbar in a meshed dc grid can change due to system reconfiguration, maintenance, or outage. Third, the conduction of surge arresters during a dc fault will also influence the voltage and current waveforms. In addition, system parameters such as breaker opening delays differ according to the breaker types and vendors.

This paper extends the method of [10] to bipolar systems and assesses the robustness of the breaker failure backup

protection algorithm against the aforementioned operating conditions and system parameters. During the time frame of interest for the backup protection, not only the travelling wave phenomenon but also the converter control, converter protection and ac in-feed can play a role in determining the fault voltages and currents. In order to incorporate all these factors, the robustness of the backup protection algorithm is evaluated via simulation studies on a detailed three-terminal bipolar test system implemented in PSCAD [15].

The remainder of this paper is organized as follows. Section 2 gives a brief introduction of the breaker failure backup protection applied in a three-terminal bipolar test system. In section 3, fault behaviour under various operating conditions is analysed. Section 4 investigates the robustness of the breaker failure backup protection algorithm using time domain simulation studies. The conclusions are given in section 5.

2 Fast breaker backup protection

2.1 Fast breaker failure backup protection algorithm

The basic backup principle proposed in [10] relies on finding a UI-threshold to distinguish uncleared and cleared faults after a presumed primary breaker opening delay t_{br}. A fault is detected by the primary protection at t_d. After the primary breaker opening delay, the primary breaker opens at t_o and starts to interrupt the fault. Once fault current interruption starts, the fault current decreases and the voltage returns to a high value. On the contrary, if the primary circuit breaker fails, the fault current continues to increase while the voltage remains low. This difference is illustrated in Fig. 1 in the UI-plane, where the arrows indicate the change of the voltage-current loci as a function of time. The dash-dotted line is the relay setting which is able to separate uncleared and cleared faults.

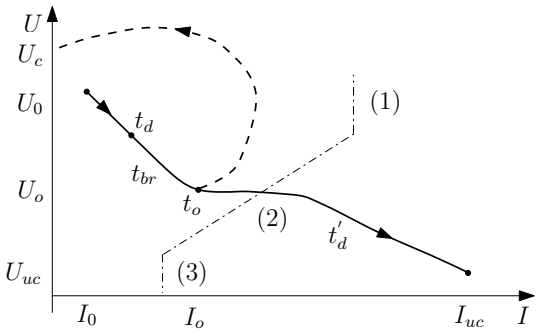

Fig. 1: Principle of the fast breaker backup protection algorithm (solid line: uncleared fault, dashed line: cleared fault, dash-dotted line: backup relay characteristic) Note. Reprinted from [10].

The UI-threshold can be trained on sampled data from off-line simulations using linear discriminant analysis (LDA). The samples are vectors of $(i(t_o + k\Delta t), u(t_o + k\Delta t))$, which are sampled between the breaker opening instant t_o and the backup protection detection instant $t_d^{'}$ with a sampling interval Δt. The sampled data are divided into two sets, X_1 and X_2 for uncleared and cleared faults, respectively. The LDA technique projects sets of samples into a direction that maximizes the separability between the two sets. The projection (one-dimensional transformed value) of the current and voltage sample is obtained by Equation (1), and the threshold is defined by the distance of the two closest transformed samples from the two sets. Further details on finding the threshold using LDA can be found in [10].

$$\begin{cases} y_k = \omega_1 i(t_o + k\Delta t) + \omega_2 u(t_o + k\Delta t) \\ y_{th} = \dfrac{y_1^d + y_2^d}{2} \end{cases} \quad (1)$$

where y_k: transformed value, $i(t_o + k\Delta t), u(t_o + k\Delta t)$: the k^{th} current, voltage sample, $\omega_{1,2}$: the slope of the direction, y_1^d and y_2^d: two closest transformed samples from uncleared and cleared faults.

2.2 Application in a three-terminal bipolar test system

Fig. 2 shows the three-terminal bipolar test system used for the studies in this paper. The system parameters and models are taken from [15], except the dc circuit breaker model and the values of the series inductors, which are taken from [10]. The breaker opening delay is assumed to be 2 ms for hybrid dc circuit breakers [10] in the reference scenario. In the pre-fault steady-state, converter station 1 and 2 export 400 MW and 600 MW, respectively to converter station 3, with power evenly shared between the positive and negative poles. As a reference case, the system is assumed to be grounded at station 3 and the neutral bus surge arresters at converter station 1 and 3 are disconnected via opening switches S_1 and S_2. Pole-to-ground faults at nine fault locations along link 13p for both successful fault clearing and breaker B_{13} failure are simulated. The faults are incepted at 0 ms in the simulation. Fig. 3 shows the UI-threshold (thr_{Ref}) trained on the samples collected from these nine fault locations which optimally separates the uncleared and cleared faults under the reference operation condition.

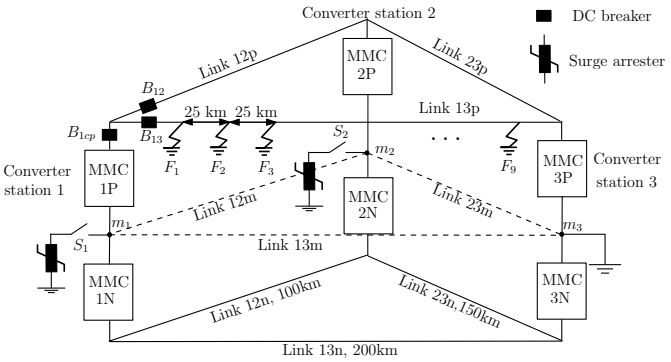

Fig. 2: Three-terminal bipolar test system.

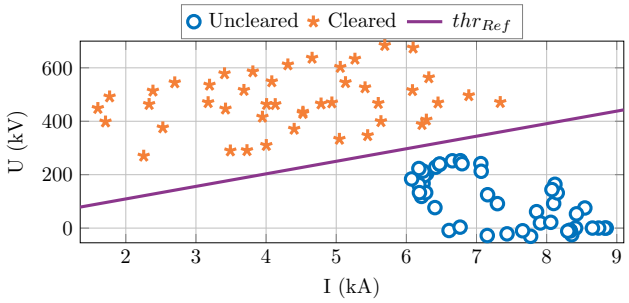

Fig. 3: Threshold determination for B_{13} breaker failure backup protection (Case Ref).

3 Dc fault behaviour under various operation conditions

One of the most important requirements on protection algorithms is the insensitivity to operation conditions and system changes. In this section, the influence of these parameters on fault behaviour is analysed using the three-terminal bipolar test system. Table 1 summarizes the cases and conditions considered in this study.

Table 1: Operating conditions considered in the study.

Cases (Suffix used in figures)	**Conditions** Power Flow [pu] @ 500 MW (+/-:inverter/rectifier)
Reference case (Ref)	P_{1p}=P_{1n}= -0.4, P_{2p}=P_{2n}= -0.6, P_{3p}=P_{3n}= 1
Maximum power flow (Pfp1)	P_{1p}=P_{1n}= 1, P_{2p}=P_{2n}= -0.4, P_{3p}=P_{3n}= -0.6
Minimum power flow (Pfn1)	P_{1p}=P_{1n}= -1, P_{2p}=P_{2n}= 0.4, P_{3p}=P_{3n}= 0.6
Unbalanced power flow (Ubpf)	P_{1n}= -1, P_{2n}= 0, P_{3n}= 1, positive pole settings are same as the reference case
Link 12p outage (LO)	same as the reference case
Arresters in service (Arr)	same as the reference case
Grounding at G1 (G1)	same as the reference case

3.1 Pre-fault power flow

Pre-fault power flow in a bipolar configuration can influence dc fault behaviour in two ways. First, the pre-fault current of a converter influences the instant of the converter blocking. Second, the unbalanced power flow in the positive and negative poles also have an impact on the fault waveforms. As shown in Fig. 4 (a), converter MMC 1p is blocked at 1.4 ms after fault inception in the case where the direction of the pre-fault converter current is same as that of the fault current. However, if the pre-fault converter current and the fault current are of opposite direction, converter MMC 1p is blocked at 3.8 ms, which is much longer compared to the previous case. During the discrimination window for the backup protection, the current contributed from the converter side could have large differences depending on the initial power flow if the instantaneous current is used for discrimination of uncleared and cleared faults.

Unlike symmetrical monopolar systems, where the currents flowing through the two poles always have equal magnitude, a bipolar configuration with metallic or ground return allows unbalanced power flow in the positive and negative poles. As discussed in [16], the existence of the metallic return path influences the mutual coupling between the two poles during both transient and steady-state phases. Fig. 5 compares the influence of unbalanced power flow in the negative pole on the fault currents and voltages. In the unbalanced power flow case (Case Ubpf), the pre-fault currents of the converter MMC 1p and MMC 1n are -0.4 pu and -1.0 pu, respectively. As shown in Fig. 5, the unbalanced power flow in the negative pole has insignificant influence on the fault voltage and current waveforms in the positive pole within the time window of interest.

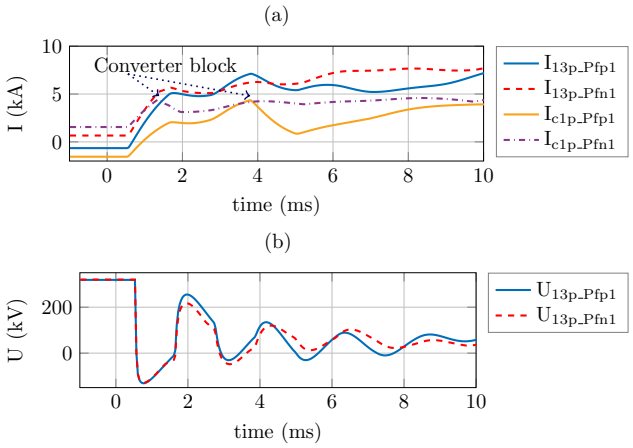

Fig. 4: Influence of pre-fault power flow on fault behaviour, Case Pfp1 and Case Pfn1: F_5 (a) currents in link 13p and MMC 1p (b) voltages of link 13p.

3.2 Number of parallel branches

The number of parallel branches mostly influence the total fault current experienced by the breaker B_{13} during a fault on link 13p. In the test system shown in Fig. 2, the fault current seen by the breaker B_{13} is mainly coming from submodule capacitive discharges of the converter MMC 1p, the discharge of the adjacent cable link 12p and ac in-feed after converter blocking. Fig. 6 compares the currents and voltages in case link 12p is out-of-service. As shown in Fig. 6, both current and voltage seen by B_{13} change significantly due to a decrease in cable discharge when link 12p is out-of-service.

3.3 Grounding location

The grounding location influences the total impedance of the converter discharging path and in turn influences the total cur-

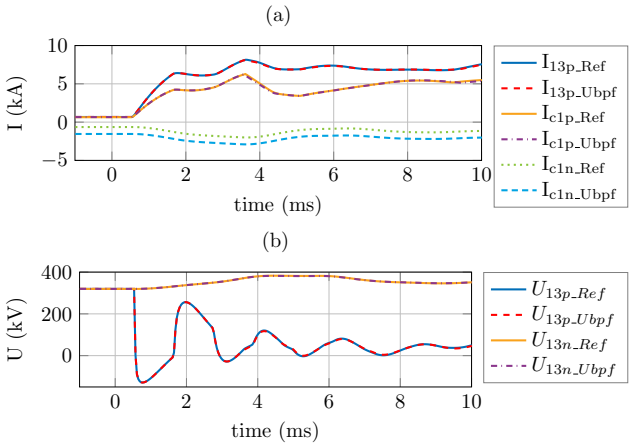

Fig. 5: Influence of unbalanced power flow on fault behaviour, Case Ref and Case Ubpf: F_5 (a) currents in link 13p, MMC 1p and MMC 1n (b) voltages of link 13p and link 13n.

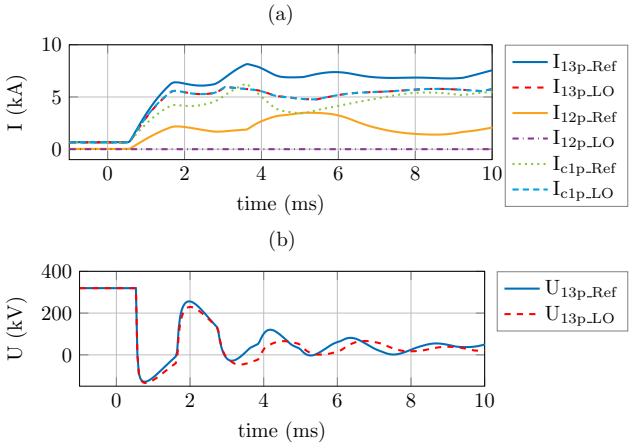

Fig. 6: Influence of number of parallel branches, Case Ref and Case LO: F_5 (a) currents in link 13p, link 12p and MMC 1p (b) voltages of link 13p.

rent seen by the breaker B_{13}. The total impedance of the discharging path is comprised of the equivalent impedance of the converter, the series inductor, and the impedance of the cable. The impedance of the cable in the discharging path is the sum of the impedance of the positive and return cable, if the grounding location is at converter station 3 and the fault location is F_9. On the contrary, this impedance is zero, if the bipolar test system is grounded at converter station 1 and the fault location is F_1. In addition, the discharging current from the adjacent cable, link 12p, also changes according to the fault location. The closer the fault location is to the converter station 1, the larger the discharge current from the adjacent cable will be. The combination of fault location F_1 and grounding location G_1 results in the largest current seen by the breaker B_{13}, and the combination of fault location F_9 and grounding location G_3 results in the lowest current. Fig. 7 (a) shows that the current difference in these two cases is about a few kA during the sampling window for the backup protection.

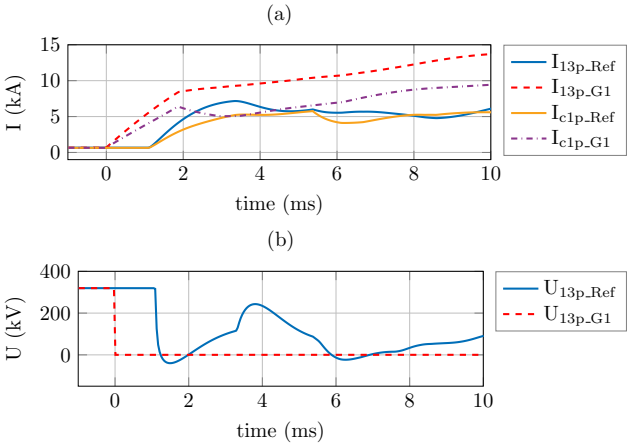

Fig. 7: Influence of grounding location, Case Ref: F_9 and Case G1: F_1 (a) currents in link 13p and MMC 1p (b) voltages of link 13p.

3.4 Operation of surge arresters

In solidly or low-impedance grounded bipolar system, the steady-state post-fault voltage on the healthy pole is the nominal voltage for a pole-to-ground fault [14]. The transient voltage in this case is not expected to be high enough to reach the operation level of the dc bus/line arresters considering that the cable is typically designed to withstand 1.85 pu during routine test and type test [18]. The transient voltages on the metallic return at the ungrounded side however could reach the operation level of the neutral bus arresters since the surge withstand level of a return cable is normally very low [14], [18]. Once the neutral bus arresters start to conduct, there will be additional temporary grounding points through these arresters. Fig. 8 (b) shows a situation where voltage at the neutral bus of converter station 1 is clamped to its protective level around 1 ms. Due to the operation of these neutral bus arresters, the magnitudes of the transient voltages and currents of the return cables and the negative pole are smaller (Fig. 8).

4 Robustness of the fast breaker backup protection

4.1 Robustness against operating conditions

The threshold trained on the reference case, thr_{Ref} is tested on pole-to-ground faults along link 13p for cases listed in Table 1 to assess the necessity of retraining the threshold. Fig. 9 compares thr_{Ref} and thr_{All}, which is the threshold trained on samples from all cases. As shown in Fig. 9, thr_{Ref} is no longer the best threshold for various operating conditions but still able to separate uncleared and cleared sampled data in all cases. Among all the conditions studied, the samples under maximum power flow condition (Case Pfp1) are the closest to thr_{Ref}. The separation margin is then evaluated for uncleared fault of fault location 7, which has the minimum transformed margin as shown in Fig. 10.

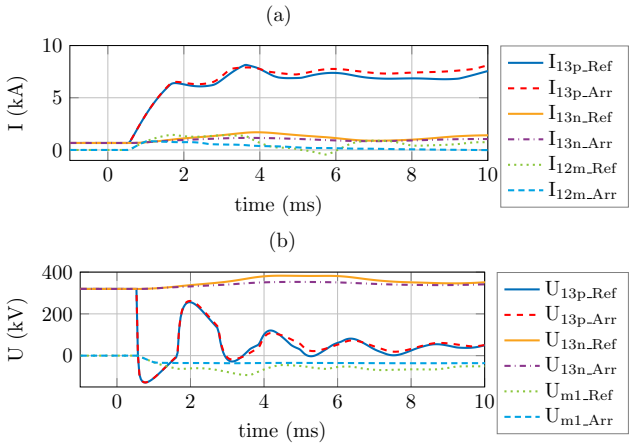

Fig. 8: Influence of surge arresters in metallic return, Case Ref and Case Arr: F_5 (a) currents in link 13p, link 13n and metallic return 12m (b) voltages of link 13p, link 13n and neutral bus m1.

The voltage and current margins are visualized in Fig. 11 and summarized in Table 2 for the worst case. The transformed margin of thr_{Ref} is 0.56 compared to 1.21 of thr_{All}. The current and voltage margin of thr_{Ref} are respectively 0.2176 pu and 0.05 pu with respect to the rated current and voltage. In actual HVDC systems, the measurement errors are typically in the order of 0.1% [19], which suggests that the UI margins of thr_{Ref} are sufficient to separate uncleared and cleared faults even taking measurement errors into consideration.

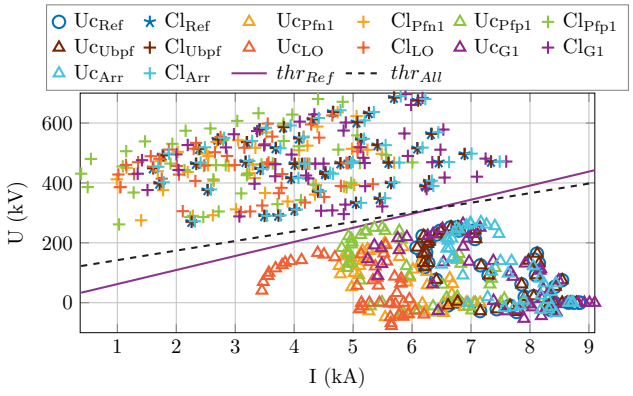

Fig. 9: Threshold determination for B_{13} breaker failure backup protection: thr_{Ref} and thr_{All} are trained on samples collected from Case Ref and all cases, respectively (Uc: uncleared, Cl:cleared).

4.2 Robustness against breaker opening delay

Hybrid and fast mechanical dc circuit breakers are considered applicable for selective protection in meshed HVDC grids. The opening delay of dc circuit breakers is in the range of 2 to 5 ms for hybrid [20], [21] and mechanical type [22]. The backup protection algorithm is then evaluated considering breaker opening delay of 3 ms and 5 ms. Since minimum power flow (Case Pfp1), unbalanced power flow (Case ubpf) and arresters

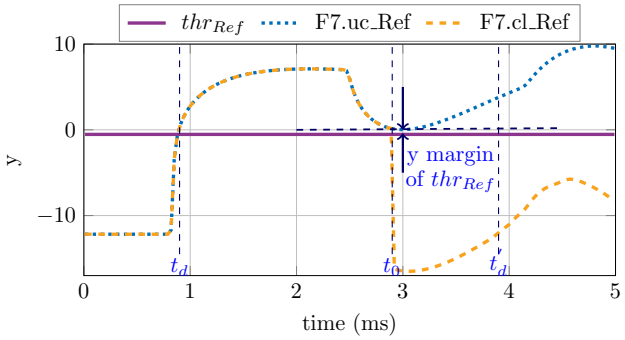

Fig. 10: Transformed samples y for the B_{13} breaker failure backup protection algorithm using thr_{Ref}, Case Pfp1: F_7.

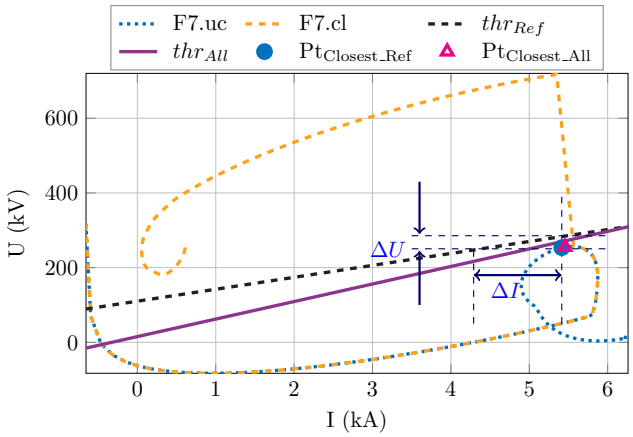

Fig. 11: Voltage and current loci for uncleared and cleared faults, Case Pfp1, Fault location F_7.

in service (Case Arr) have insignificant influences on the fault behaviour during the sampling window of the backup protection algorithm, these conditions are not taken into consideration for robustness studies against breaker opening delay.

The trained UI-thresholds for breaker opening delay of 3 ms and 5ms are shown in Fig. 12 and Fig. 14, respectively. The transformed samples and separation margins to UI-thresholds are shown in Fig. 13 and Fig. 15, respectively. Fig. 12 and Fig. 14 show that the threshold trained on the reference case can still separate uncleared and cleared sampled data in all cases for both breaker opening delays. As shown in Fig. 13, for a breaker opening delay of 3ms, the samples with F_9 under maximum power flow condition (Case Pfp1) are the closest to thr_{Ref_3ms} and thr_{All_3ms}. For breaker opening delay of 5ms, the closest sample to thr_{Ref_5ms} is fault location 7 with outage of link 12p (Case LO), while the closest sample to thr_{All_5ms} is fault location 7 with grounding location G1 (Case G1). Numeric evaluations for the transformed and UI margins are summarized in Table 2. Table 2 shows that longer breaker opening delay results in larger margins for the backup protection to discriminate between uncleared and cleared faults.

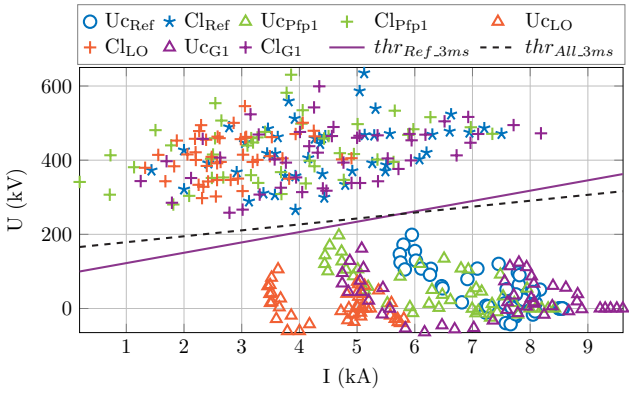

Fig. 12: Threshold determination for B_{13} breaker failure backup protection, Breaker opening delay $t_{br} = 3ms$: thr_{Ref_3ms} and thr_{All_3ms} are trained on samples collected from Case Ref and all cases, respectively (Uc: uncleared, Cl:cleared).

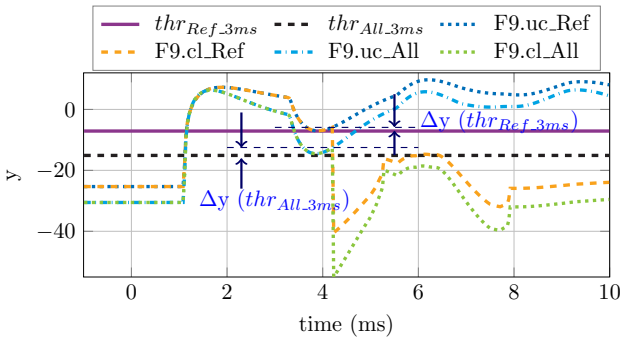

Fig. 13: Case Pfp1, Fault location F_9: transformed samples and separation margins to UI-thresholds ($\Delta y(thr_{Ref\_3ms})$ and $\Delta y(thr_{All\_3ms})$ are the separation margins to thr_{Ref_3ms} and thr_{All_3ms}, respectively).

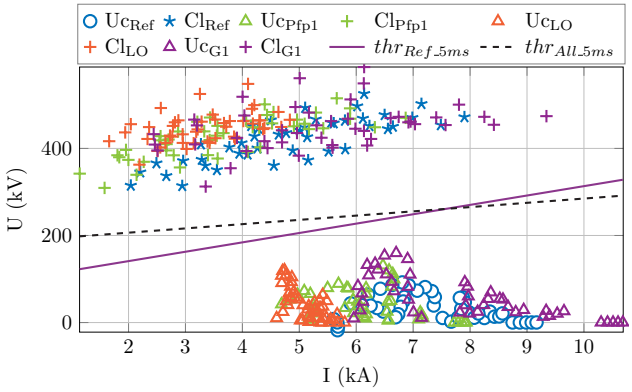

Fig. 14: Threshold determination for B_{13} breaker failure backup protection, Breaker opening delay $t_{br} = 5ms$: thr_{Ref_5ms} and thr_{All_5ms} are trained on samples collected from Case Ref and all cases, respectively (Uc: uncleared, Cl:cleared).

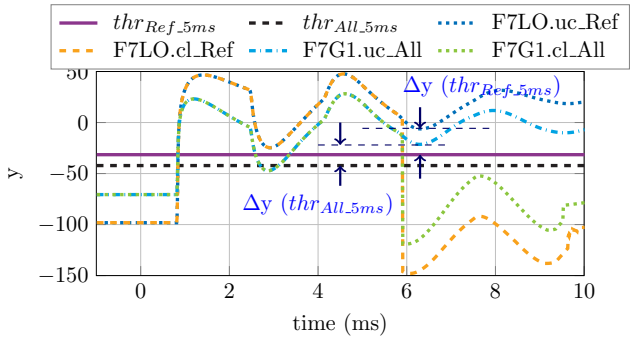

Fig. 15: Case LO and Case G1, Fault location F_7: transformed samples and separation margins to UI-thresholds ($\Delta y(thr_{Ref\_5ms})$ and $\Delta y(thr_{All\_5ms})$ are the separation margins to thr_{Ref_5ms} and thr_{All_5ms}, respectively).

Table 2: Margin of y and UI-thresholds.
Voltage base: 320 kV, Current base: 1.56 kA

Breaker Opening Delay (t_{br})		**2 ms**	**3 ms**	**5 ms**
thr_{Ref}	Closest Case, F_{no}	Pfp1,F_7	Pfp1,F_9	LO,F_7
	Δy	0.56	1.28	25.27
	ΔU [pu]	0.0503	0.0533	0.2458
	ΔI [pu]	0.2176	0.3914	2.3386
thr_{All}	Closest Case, F_{no}	Pfp1,F_7	Pfp1,F_9	G1,F_7
	Δy	1.21	2.60	20.78
	ΔU [pu]	0.0919	0.0877	0.2877
	ΔI [pu]	0.5888	1.1241	6.0130

5 Conclusion

This paper studied the applicability of a fast breaker failure backup protection algorithm to protect bipolar HVDC grids and evaluated the robustness of the backup protection algorithm against various operation conditions and breaker opening delays. The simulation results demonstrate the robustness of the UI-thresholds in the bipolar test system, considering initial power flow, number of parallel branches, grounding location, and surge arresters. If the UI-threshold is trained based only on one specific condition, the margin of this threshold is reduced when distinguishing uncleared and cleared faults under different operating conditions. However, the UI-threshold trained on a reference case is still able to separate uncleared and cleared faults under all conditions considered in this study, which suggests that it is not required to retrain the threshold for different operating conditions. The voltage and current margins of the threshold are found to be sufficient even taking measurement errors into consideration. In addition, the UI-threshold is also robust against breaker opening delays. Longer breaker opening delays result in larger margins for the backup protection to operate.

Acknowledgements

The work of M. Wang and W. Leterme is funded by Horizon 2020 PROMOTioN project (Progress on Meshed HVDC Offshore Transmission Networks) under grant agreement No 691714. The work of Jef Beerten is funded by a research grant of the Research Foundation-Flanders (FWO).

References

[1] D. Van Hertem, M. Ghandhari, J. B. Curis, O. Despouys, and M. Andrée, "Protection requirements for a multi-terminal meshed DC grid," in *Proc. Cigré Bologna Symp.*, Bologna, Italy, 13–15 Sep. 2011, 8 pages.

[2] P. M. Anderson, *Power System Protection*. Hoboken, NJ, USA:: J. Wiley & Sons, 1998.

[3] K. De Kerf, K. Srivastava, M. Reza, D. Bekaert, S. Cole, D. Van Hertem, and R. Belmans, "Wavelet-based protection strategy for DC faults in multi-terminal VSC HVDC systems," *IET Gener. Transm. Distrib.*, vol. 5, no. 4, pp. 496–503, Apr. 2011.

[4] W. Leterme, J. Beerten, and D. Van Hertem, "Non-unit protection of HVDC grids with inductive dc cable termination," *IEEE Trans. Power Del.*, vol. 31, no. 2, pp. 820–828, Apr. 2016.

[5] J. Sneath and A. D. Rajapakse, "Fault Detection and Interruption in an Earthed HVDC Grid using ROCOV and Hybrid DC Breakers," *IEEE Trans. Power Del.*, vol. 31, no. 3, pp. 973–981, Jun. 2016.

[6] N. Johannesson, S. Norrga, and C. Wikström, "Selective Wave-Front Based Protection Algorithm for MTDC Systems," in *Proc. IET DPSP 2016*, Edinburgh, UK, 7–10 Mar. 2016, 6 pages.

[7] J. Descloux, "Protection contre les courts-circuits des réseaux à courant continu de forte puissance," Ph.D. dissertation, Université de Grenoble, Grenoble, France, Sep. 2013.

[8] N. Johannesson and S. Norrga, "Longitudinal differential protection based on the Universal Line Model," in *Proc. Industrial Electronics Society, IECON 2015 - 41st Annual Conference of the IEEE*, Yokohama, Japan, 9-12 Nov. 2015, pp. 001 091–001 096.

[9] M. Hajian, Lu Zhang, and D. Jovcic, "DC transmission grid with low speed protection using mechanical DC circuit breakers," *IEEE Trans. Power Del.*, vol. 30, no. 3, pp. 1383–1391, Jun. 2015.

[10] W. Leterme, S. P. Azad, and D. Van Hertem, "Fast Breaker Failure Backup Protection for HVDC Grids," in *Proc. IPST 2015*, Cavtat, Croatia, 15-18 Jun. 2015, 6 pages.

[11] W. Leterme, S. P. Azad, and D. Van Hertem, "A Local Backup Protection Algorithm for HVDC Grids," *IEEE Trans. Power Del.*, vol. 31, no. 4, pp. 1767–1775, Aug. 2016.

[12] Cigré Working Group B4.52, "HVDC Grid Feasibility Study," *Cigré Techinical Brochure*, Apr. 2013.

[13] S. De Boeck, P. Tielens, W. Leterme, and D. Van Hertem, "Configurations and earthing of HVDC grids," in *Proc. IEEE PES GM 2013*, Vancouver, Canada, 21–25 July 2013, 5 pages.

[14] W. Leterme, P. Tielens, S. De Boeck, and D. Van Hertem, "Overview of grounding and configuration options for meshed HVDC grids," *IEEE Trans. Power Del.*, vol. 29, no. 6, pp. 2467–2475, Dec. 2014.

[15] M. Wang, J. Beerten, and D. Van Hertem, "DC Fault Analysis in Bipolar HVDC Grids," in *Proc. IEEE YRS 2016. IEEE Benelux PELS/PES/IAS Young Researchers Symposium*, Eindhoven, Netherlands, 12–13 May 2016, 6 pages.

[16] C. Berto, "Modelling and power-voltage control in unbalanced bipolar multi-terminal HVDC grids," Master's thesis, Universit‘ a degli Studi di Padova, Padova, Italy, Jun. 2016.

[17] F. B. Ajaei and R. Iravani, "Cable Surge Arrester Operation Due to Transient Overvoltages Under DC-Side Faults in the MMC-HVDC Link," *IEEE Trans. Power Del.*, vol. 31, no. 3, pp. 1213–1222, Jun. 2016.

[18] Cigré Working Group B1.32, "Recommendations for Testing DC Extruded Cable Systems for Power Transmission at a Rated Voltage up to 500 kV," *Cigré Techinical Brochure*, Apr. 2012.

[19] F. Jenau and G. Testin, "Modern Instrument Transformer Technologies for UHVAC and HVDC Networks," in *Proc. CIGR India Symp.* New Delhi, India, 29-30 Jan. 2009, 16 pages.

[20] J. Häfner and B. Jacobson, "Proactive hybrid hvdc breakers-a key innovation for reliable hvdc grids," in *Proc. Cigré Bologna Symp.*, Bologna, Italy, 13–15 Sep. 2011, 8 pages.

[21] C. C. Davidson, R. S. Whitehouse, C. D. Barker, J.-P. Dupraz, and W. Grieshaber, "A new ultra-fast HVDC Circuit breaker for meshed DC networks," in *Proc. IET ACDC*, Birmingham, UK, 10-12 Feb. 2015, 7 pages.

[22] K. Tahata, S. El Oukaili, K. Kamei, D. Yoshida, Y. Kono, R. Yamamoto, and H. Ito, "HVDC circuit breakers for HVDC grid applications," in *Proc. AORC-CIGRE 2014*, Tokyo, Japan, 27–29 May 2015, 9 pages.